Tuning Deposition Conditions for VN Thin Films Electrodes for Microsupercapacitors: Influence of the Thickness

Allan Lebreton, Jérémy Barbé, Christophe Lethien, Jonathan N Coleman, Thierry Brousse

OPEN ACCESS

Tuning Deposition Conditions for VN Thin Films Electrodes for Microsupercapacitors: Influence of the Thickness

To cite this article: Allan Lebreton *et al* 2024 *J. Electrochem. Soc.* **171** 090513

Journal of The Electrochemical Society, 2024 **171** 090513

Tuning Deposition Conditions for VN Thin Films Electrodes for Microsupercapacitors: Influence of the Thickness

Allan Lebreton,[1,2] Jérémy Barbé,[1,2,z] Christophe Lethien,[2,3,4] Jonathan N. Coleman,[5,z] and Thierry Brousse[1,2,*,z]

[1]*Nantes Université, CNRS, Institut des Matériaux de Nantes Jean Rouxel, IMN, F-44000 Nantes, France*
[2]*Réseau sur le Stockage Electrochimique de l'Energie (RS2E), CNRS FR 3459, 80039 Amiens Cedex, France*
[3]*Institut d'Electronique, de Microélectronique et de Nanotechnologies, Université de Lille, CNRS, Université Polytechnique Hauts-de-France, UMR 8520 - IEMN, F-59000 Lille, France*
[4]*Institut Universitaire de France (IUF), Saint-Michel 103, 75005, Paris, France*
[5]*School of Physics, CRANN and AMBER Research Centres, Trinity College Dublin, Dublin 2, Ireland*

Vanadium nitride is a highly promising material for micro-pseudocapacitors when used as a bifunctional thin film, i.e. an electrode material and a current collector, owing to its remarkable electrical and electrochemical properties. However, the specific limitations associated with high-rate cycling remain unclear. In this study, we evaluate how the characteristic time associated with charge/discharge of vanadium nitride films is modified with the film thicknesses using electrochemical impedance spectroscopy and cyclic voltammetry measurements coupled to a semi-empirical model commonly utilized to assess the high-rate behaviour of battery electrodes. Both methodologies are in good agreement and revealed that rate capability of this bi-functional material is limited by the VN electrical conductivity. To confirm this finding, VN thin films were sputtered on platinum current collectors, leading to a six-fold reduction in the characteristic time associated with charge/discharge of the current collectors/electrode material. This underscores the importance of using current collectors even for highly conductive electrode materials.
 [DOI: 10.1149/1945-7111/ad75be]

Manuscript submitted July 26, 2024; revised manuscript received August 29, 2024. Published September 11, 2024.

Supplementary material for this article is available online

Since almost two decades, vanadium nitride has been studied as potential electrode material for supercapacitors and microsupercapacitors.[1–6] The synthesis of nanosized VN powder is often challenging and difficult to scale up. This is the main reason why most of the research works has been dedicated to the deposition of VN thin films.[7–10] Indeed, VN coatings are commonly used in various domains such as cutting and drilling tools.[11] Moreover, the deposition of such coating often takes place via physical vapour deposition techniques such as reactive DC sputtering, using a metallic vanadium target and nitrogen as the reactive gas. Such techniques are highly compatible with microelectronic processes which makes it possible to prepare interdigitated VN based electrodes implemented in microsupercapacitor applications Last, the synthesis of a solid-state electrolyte has been developed which enables the fabrication of all solid state microdevices with quite interesting performances.

From a fundamental point of view, the charge storage mechanism of VN have been investigated and the predominant pseudocapacitive charge storage has been evidenced,[4,8,9,12] although at fast charging/discharging regimes the capacitive double layer process brings an additional significant contribution to the overall capacity of the electrodes.

Our previous studies aimed at investigating the influence of the deposition conditions[9,12] on the electrochemical performances of VN thin film electrodes, complex deposition procedures were used, which will not be compatible with high production rates. Here, we have studied more basic sputtering deposition process, using room temperature and standard deposition pressures in order to demonstrate the feasibility of large-scale manufacturing processes. As fast charging/discharging regimes are expected for microsupercapacitors, similarly to what is achieved for their bulk counterpart, the balance of areal capacitance and characteristic time associated with charge/discharge is a major issue for achieving usable electrodes. Two main parameters have been identified for standard sputtering process: the polarisation of the substrate and the thickness of the deposited layer. For clarity purpose, the study of these two parameters have been divided in two parts. For each part, we use the model developed by Coleman et al. to fit experimental data,[13–16] thus leading to the determination of electrochemical properties such as the maximum capacity of the electrodes and their characteristic time associated with charge/discharge. A similar formalism can be found on,[17] presented by Fontaine et al. using mathematica software. Although this model has been used for bulk composite electrodes dedicated to battery or supercapacitor applications, its use for thin film electrodes has been investigated in the present studies. The results provided by the model further helps to propose practical solutions for optimizing VN electrodes in microsupercapacitor designs.

Material and Methods

Reactive sputtering.—VN thin films were deposited by reactive magnetron sputtering (Ar/N_2) from a pure 4′ vanadium target (99.9% purity from NEYCO) using a magnetron reactor from MHS with three 4′ targets in confocal configuration. Quarters of 4′ Si wafer with 500 nm thermal oxide layer from CODEX were cleaned with ethanol and acetone prior to deposition. A 3×3 cm mask was fixed on the wafer in order to control the deposition region. Before deposition, residual pressure was kept below 10^{-6} mbar and the target-substrate distance was fixed at 15 cm. A pre-sputtering step of the target is performed before the deposition: a pure Ar plasma was ignited at 300 W to clean and deoxidize the target surface for 3 min. Then, N_2 was introduced into the chamber and the shutter was opened. During thin film deposition, argon flow rate was fixed at 80 sccm and the substrate was not intentionally heated. The nitrogen flow was fixed at 1.6 sccm and sputtering power at 100 W. Pressure was set at 5.10^{-3} mbar during the sputtering process. For all depositions, polarisation of the substrate holder was fixed at −80 V and the substrate holder was rotating at 10 rpm staying in the center of the deposition region during the hole deposition. The deposition time was modified from 38 min to 497 min to tune the film thicknesses from 50 to 580 nm respectively

*Electrochemical Society Member.
[z]E-mail: jeremy.barbe@univ-nantes.fr; COLEMAJ@tcd.ie; thierry.brousse@univ-nantes.fr

thickness was measured using both SEM images and profilometer. Taking into account the pyramids in surface, the error is from ±5 nm for the 50 nm thick film to ±20 nm for the 580 nm thick film. Although there is no intentional introduction of molecular O_2 in the reactor, films contain a significant fraction of oxygen, which is explained by oxidation during exposure to air, due to the high getter property of vanadium and porosity of the films.[18] This is why the obtained VN thin films also contain a significant fraction of amorphous vanadium oxide. Our results suggest that the films are composed of these two distinct phases. However, for simplicity reasons the films will be identified as VN thin films in this work. More information regarding characterization of those thin films are available in Ref. 18.

For the last part, two samples were prepared: the first one with VN films sputtered on top of a 50 nm thick platinum current collector deposited on Si/SiO_2 substrate, and the second one with VN films sputtered directly on Si/SiO_2 substrate. Platinum current collector was sputtered in AC450 reactor from Alliance Concept from a 2′ platinum target (99.9%). Sputtering power was fixed at 150 W and Ar flow at 50 sccm for a sputtering time of 45 s which lead to a final thickness of ≈50 nm.

Thin film characterization.—Room temperature XRD data were obtained using a Bruker "D8 Advance" diffractometer operated in Bragg-Brentano geometry with a Cu anode sealed X-ray tube and a focusing Ge(111) primary monochromator (selecting the Cu Kα1 radiation; $\lambda = 1.540598$ Å). We used a 1-D silicon-strip position sensitive detector ("LynxEye" detector) with an active area of 3.7° 2Θ (goniometer radius: 217.5 mm).

SEM measurements were conducted on a ZEISS Merlin instrument, in secondary electron configuration at 20 kV and 100 Pa. For SEM measurements, size of the pyramids was determined using imageJ software on a basis of the mean value of 10 measurements. Cross sections were made by cleaving the substrate under air atmosphere with a diamond tip.

The apparent density of deposited materials was measured using a microbalance (0.1 mg precision) and knowing the thickness and surface area of thin films deposited through a 3×3 cm^2 mask during deposition.

Conductivity measurement were performed in order to obtain the in-plane conductivity, by 4-point probe method using a pro4 device from Lucas Labs connected with a Keithley 2601 A system sourcemeter. The software used to run those experiments was Pro4 and the measurements were performed applying a current of 10 mA with a 5% tolerance.

Electrochemical measurements.—Electrochemical measurements were performed in 1 M KOH aqueous electrolyte using a flat cell in a three electrode configuration. The measurement zone is a circle of 0,8 mm diameter, leading to an electrochemically active area of 0,502 cm^{-2}, the crocodile pinch is fixed around 1 cm from the circle center. All measurements were conducted at a temperature of 295 K. Hg/HgO was used as reference electrode and a platinum wire as the counter electrode. Nitrogen bubbling was carried out prior to measurement to eliminate dissolved O_2 from the electrolyte. VMP3 potentiostat/galvanostat (Biologic) monitored by EC-lab software, was used for data collection and data processing. The electrochemical protocol used to characterize the films was the same for all samples, 50 activation cycles at 20 $mV.s^{-1}$ were performed before measurements. The potential window was fixed between −1 V and −0.4 V vs Hg/HgO reference electrode to avoid any side reaction and/or additional sample degradation.[19] CV measurements were realised with scan rates ranging from 10 to 10 000 $mV.s^{-1}$. Electrochemical Impedance Spectroscopy measurements were performed at open circuit voltage (OCV) and an AC signal (amplitude of 10 mV) with frequency range between 100 mHz and 1 MHz is superimposed to the static OCV signal.

Results and Discussion

Thin films morphology and microstructure.—VN thin films were deposited via reactive DC magnetron sputtering with sputtering time varying from 38 min to 497 min in order to cover a range of thicknesses from 50 nm to 580 nm. Samples present a columnar structure, as shown in Fig. 1. The top of the columns tends to merge when the thickness increases, as observed in Figs. 1c and 1d. Therefore, pyramids observed on the surface increase in size from 18 nm to 180 nm with increasing thickness. These pyramids correspond to the tops of the columns and are directly correlated with the column size, which widens with increasing thicknesses.

Cross-sectional and top-view images indicate that the samples are porous (Fig. 1). A closer examination (Figs. S1 in SI) reveals both intercolumnar and intracolumnar porosities, consistent with previous work on sputtered vanadium nitride thin films.[9,12,20] The high magnification top-view image of sample sputtered for 497 min, presented in Fig. S1, shows that pyramids are composed of sheets of VN on the surface, which suggests competitive growth of crystallites with different preferential orientations, leading to the highly porous hierarchical microstructures.

Density was measured by weighing samples before and after the VN deposition, knowing the thickness and the surface of the films deposited through a mask (3×3 cm). Results are presented in Fig. 2a. Density remains stable around 4.5 $g.cm^{-3}$ as thickness

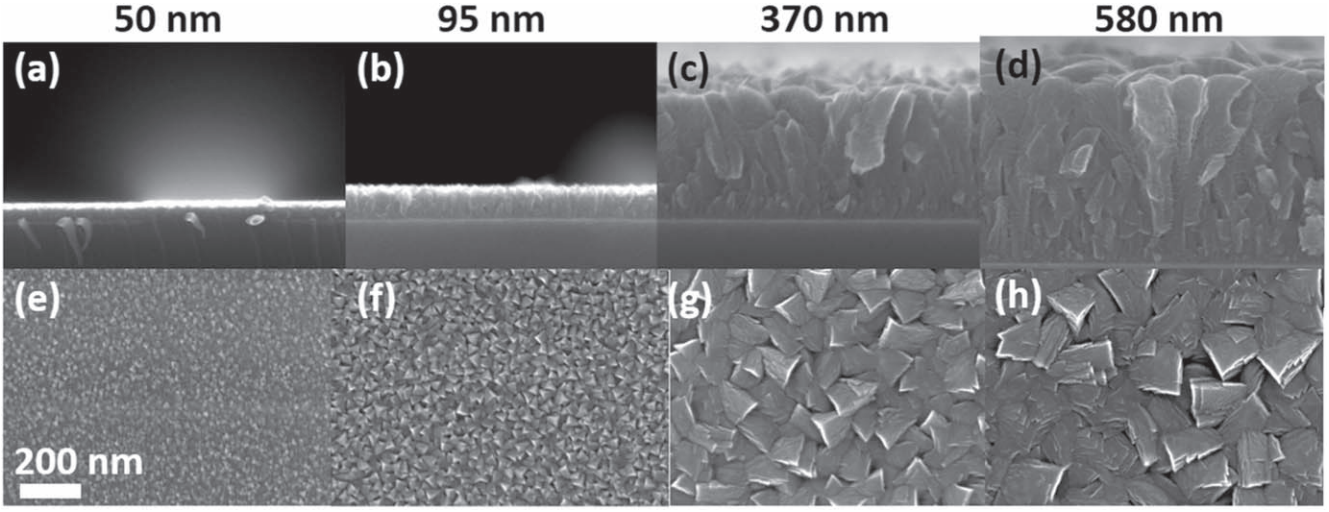

Figure 1. SEM images of cross-section and surface of vanadium nitrides thin films sputtered of (a), (e) 50 nm, (b), (f) 95 nm, (c), (g) 370 nm and (d), (h) 580 nm thin films.

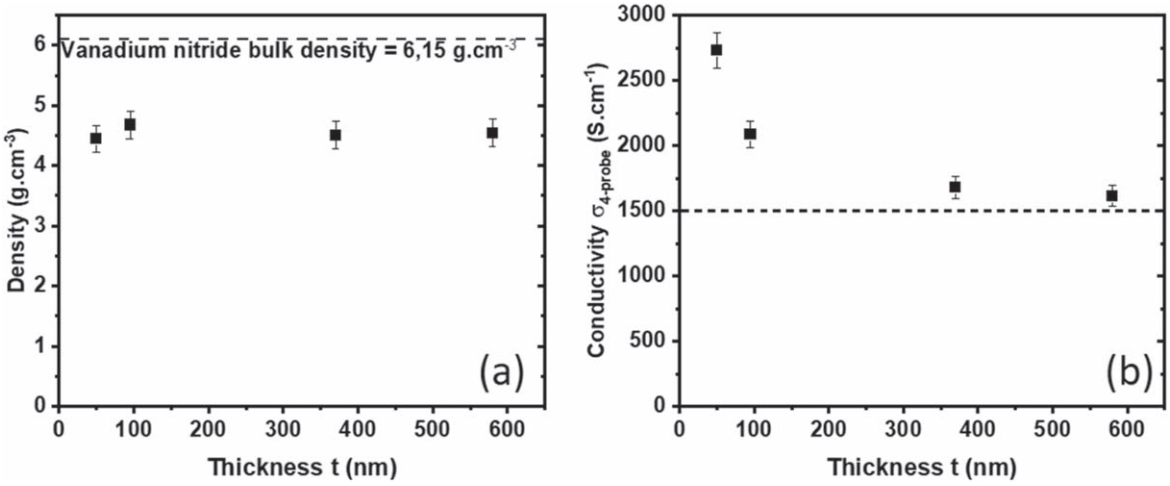

Figure 2. Vanadium nitride thin film (a) density and (b) electronic conductivity (measured using 4-point probe) as a function of thickness. Dashed line in (b) is a guideline for the eyes emphasizing the plateau reached for electronic conductivity when increasing film thickness.

increases, indicating constant porosity across the thickness range of 0–600 nm. The film compacity is approximately 75% (using 6.15 g.cm^{-3} as the density of pure and dense vanadium nitride), suggesting that approximately 25% of the film volume is composed of voids.

Four-point probe measurements were conducted to obtain the in-plane conductivity, with results presented in Fig. 2b. The in-plane conductivity ($\sigma_{4\text{-probe}}$) decreases from 2750 S.cm^{-1} to 1500 S.cm^{-1} with increasing thickness. Those values are notably lower than the bulk conductivity of VN (σ_{bulk} = 16700 S.cm^{-1}[21,22]). Multiple parameters have to be considered to explain this difference. First, the inter-columnar void increases the tortuosity and lateral electronic pathway and leads to a decrease of the in-plane conductivity as compared to bulk material. Second, those samples are polycrystalline with small crystallites size ranging from 10–30 nm and contain a significant amount of grain boundaries, which in turn hinder electronic conductivity.[18] Finally, we previously showed that these films are not composed of pure VN but contain a high amount (10–30 at%) of oxygen, which will also decrease the electronic conductivity as vanadium oxides exhibit higher resistance than vanadium nitrides.[18]

Electrochemical performance of vanadium nitride films.—The electrochemical behaviour of vanadium nitride films was first investigated using cyclic voltammetry. The scan rates were varied from 1 mV.s^{-1} to 10000 mV.s^{-1}. The results depicted in Fig. 3 reveal distinct electrochemical signatures.[23] At lower scan rates (Figs. 3a, 3b), the films exhibit a characteristic rectangular shape envelope, indicative of capacitive and/or pseudocapacitive behaviour, on which is superimposed a pair of broad redox peaks centered at −0.65 V vs Hg/HgO. Notably, this redox feature manifests only with significant film thicknesses, typically exceeding 95 nm. The observed shift between reduction and oxidation peaks increases with scan rate, and a transition to resistive behaviour is observed at 1000 mV.s^{-1} (Fig. 3c). At the highest scan rate of 10,000 mV.s^{-1} (Fig. 3d), the cyclic voltammograms do not present pseudo-capacitive or faradaic properties, indicating a transition to a resistor-like response at such fast scan rates.

Impedance spectroscopy measurements have been carried out on vanadium nitride films to extract further information on the charge storage processes, particularly focusing on what we define as the characteristic time associated with charge/discharge τ of the electrodes. This parameter describes the minimum cycle duration or minimum time at which the sample can be cycled while still exhibiting a capacitive/pseudocapacitive behaviour, whereas at higher rates, the sample is limited by various factors, such as diffusion and/or electrical limitations, leading to a resistive behaviour as clearly shown in Fig. 3d. In this study, τ is attributed to the timescale (inverse of rate) at which the rates of energy dissipation and storage within the same are the same, corresponding to the transition time between capacitive and resistive behaviour.[23] The characteristic time associated with charge/discharge can be measured in two ways, from the EIS spectrum (τ_{EIS}) and by fitting the capacitance vs scan rate data explained below, (τ_{fit}).

We measured impedance spectra for our VN films of various thickness and plotted the real and imaginary impedance as Nyquist plots in Fig. 4a. These curves are consistent with an equivalent circuit consisting of a resistor in series with a constant phase element (CPE). These curves were fit using EC-lab software (Z_{fit}) and the resistance, and the CPE constant are presented in Figs. 4b, 4c. We can easily identify the decrease of thin film resistance as well as increase in CPE constant with increasing film thickness, which was expected because of the increase in the amount of active material.

We fit the data in Fig. 4a assuming a series R-CPE combination. We believe the physical origin of R_{EIS} is the resistance associated with current flowing through the VN to get to the VN-electrolyte interface. Because we have not used a current collector, this resistance is dominated by the lateral current flow from the contact at the side of the VN to the centre of the electrochemically active region over a distance L. We can test this by calculating the associated electronic conductivity:

$$\sigma_{EIS} = R_{EIS}^{-1}\, L/W$$

where W is the width of the active region and t is the film thickness. In Fig. 4d, we plot the electronic conductivity values obtained in this way vs those found using 4-point probe measurements, $\sigma\sigma_{4\text{probe}}$. These conductivities are linearly proportional to each other with a slope very close to 1, indicating that $\sigma_{4\text{probe}} = \sigma_{\text{EIS}}$. This is strong evidence that these supercapacitors are consistent with a series R-CPE combination. The same verification was made regarding capacitance values and is presented in SI indicating a linear correlation between capacitance obtained using EIS and using semi-empirical method presented later on.

We can use the impedance data to calculate a characteristic time associated with charge/discharge describing the transition from capacitive to resistive behaviour. This is achieved by analysing the imaginary part of the complex capacitance vs frequency, as described in Ref. 24. We first converted our data to Bode plots, i.e. the C′ (imaginary) (Eq. 1) vs the frequency plots, as shown in Fig. 4e, using

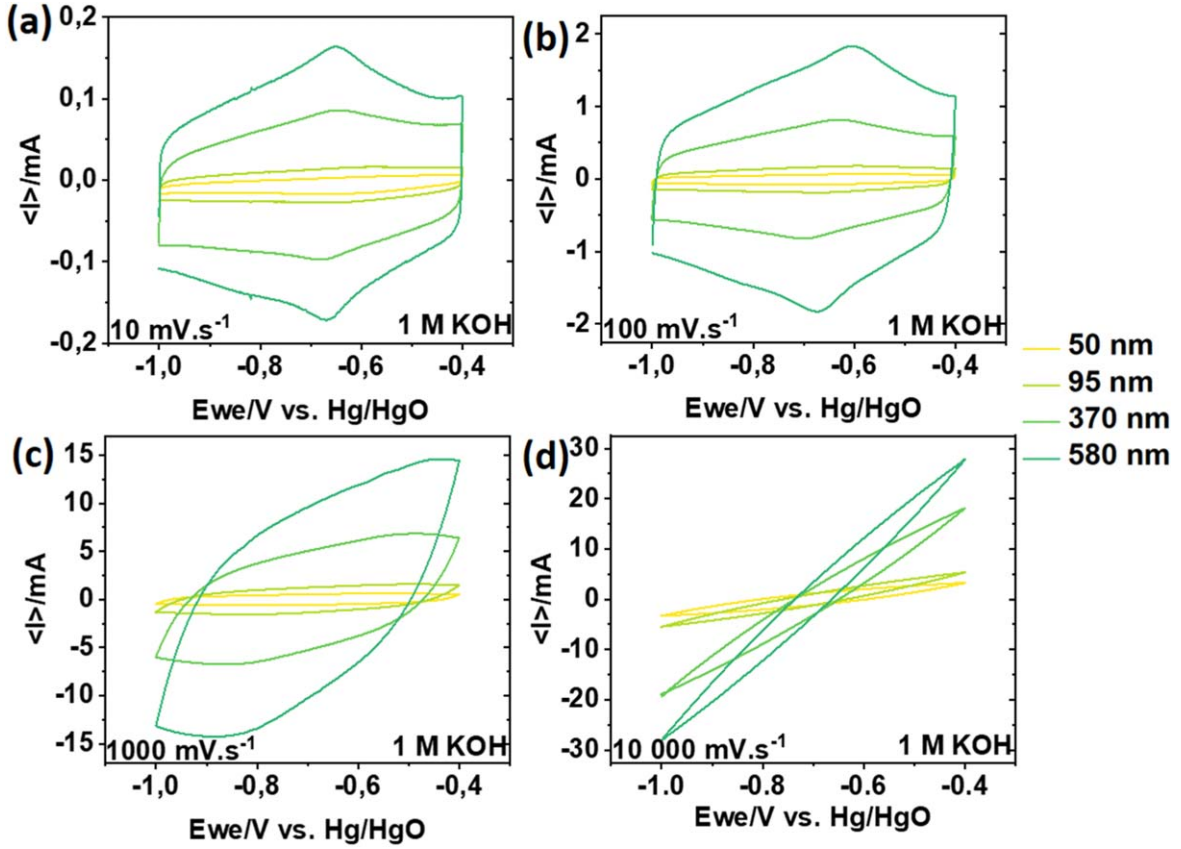

Figure 3 Cyclic voltammograms of vanadium oxynitride thin films between −1 V and −0.4 V vs Hg/HgO in 1 M KOH cycled at (a) 10 mV.s^{-1}, (b) 100 mV.s^{-1} and (c) 1000 mV.s^{-1} and (d) 10 000 mV.s^{-1}.

$$C''(\omega) = \frac{Z'(\omega)}{\omega\,|Z(\omega)|^2} \quad [1]$$

For a series R-CPE circuit, the peak position in the C′ vs frequency plot corresponds to the frequency, f_0, which defines a characteristic time associated with charge/discharge $\tau_{EIS} = 1/f_0$. This characteristic time describes the time constant associated with the transition from capacitive to resistive behaviour. The resultant times are plotted in Fig. 4f, and show that a noticeable trend emerges where the characteristic time associated with charge/discharge τ_{EIS} increases from 0.17 to 0.46 s with sample thickness.

It is interesting to see that the samples that are presenting the most capacitive behaviour at high rates in Fig. 3, i.e. the thickest films, are the ones presenting the lowest resistance here in Fig. 4b. This observation could indicate a close link between the high rates cycling limitations and the RC time constant.

Modelling of the rate performance.—We then examined the charge storage properties of vanadium nitride electrodes in more details by plotting the areal charge density Q (C.cm^{-2}) as a function of scan rate R (cycles.h^{-1}) for electrodes with different thicknesses (Fig. 5). The scan rate is defined by R=$\nu/\Delta V$, where ν is the potential ramp rate (mV.h^{-1}) and ΔV is the potential window (mV). To obtained more quantitative information, these curves were then fitted by a semi-empirical model described in detail in Ref. 7–10. The fitting equation is presented in Eq. 2.

$$Q_{exp} = Q_M[1 - (R\tau_{fit})^n(e^{-(R\tau_{fit})^{-n}})] \quad [2]$$

In this equation, Q_{exp} corresponds to the measured areal charge, Q_M to the maximum charge at low scan rates. R is defined as the rate in cycle/h and calculated using R = (3600 x ν)/ΔV, where ν is the scan rate in mV.s^{-1} and ΔV is the potential window of a full cycle in mV.s^{-1}. τ_{fit} is ascribed to the characteristic time associated with charge/discharge of the sample in hour/cycle obtained from the fit using Eq. 3. Finally, n characterise the power law decay at high cycling rates, and should depend on the rate-limiting mechanisms, with diffusion-limited electrodes displaying n = ½ and resistance-limited behaviour displaying n= 1. By fitting Eq. 2 to the experimental results for Q_{exp} vs R, this model allows us to obtain the three parameters previously mentioned, i.e. Q_M, τ_{fit} and n.

The fits obtained using the model are very satisfactory as can be seen from Fig. 5a. It is worth noting that for clarity of the fit, the *x*–axis must be defined as the number of cycles per hour using a log scale and the *y*–axis as the logarithm of the maximum charge stored Q_M.

The maximum areal charge Q_M vs sample thickness, t, is presented in Fig. 5b and indicates an increase of maximum charge from 0.78 mC.cm^{-2} up to 16.5 mC.cm^{-2} when thickness increases. This increase in maximum charge can be fitted linearly with a slope coefficient of 0.0259 mC.cm^{-2}.nm^{-1} (which corresponds to 259 C.cm^{-3}, 4.3 × 10^2 F.cm^{-3} or 57.1 C.g^{-1}), indicating that within the limits of the investigated thickness range the entire film depth is used to store charges homogeneously.

The exponent n describes the high-rate drop-off in capacity, which corresponds to the slope after the inflexion point vs sample thickness. An increase of this value from 0.64 to 1.06 is observed with increasing thicknesses (Fig. 5c). Usually, those values are located between 0.5 and 1, indicating diffusion or resistive limitations at high cycling rate, respectively.[13–16] The value found for the 50 nm thick sample may not be meaningful as in this case the range of scan rates is not large enough, even though measurements until 10 000 mV.s^{-1} were recorded. However, for all other samples, n values are close to 1 indicating resistive limitations.

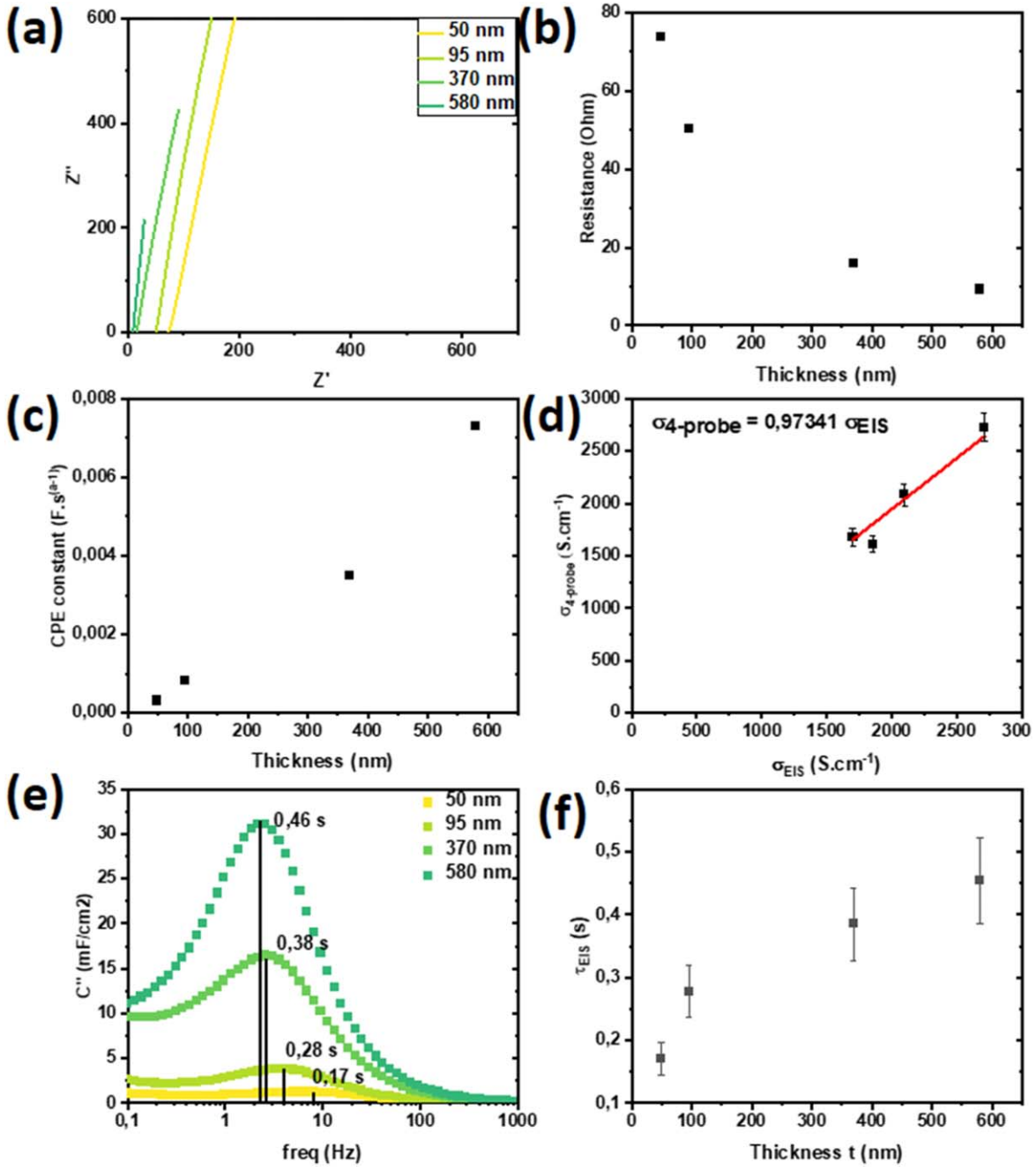

Figure 4. (a) Nyquist plot obtained from EIS measurement between 100 mHz and 1 MHz, (b) resistance obtained using Z_{fit} option from EC-lab vs thin films thickness. (c) Evolution of imaginary capacitance vs frequency and (d) evolution of τ_{fit} value vs sample thickness. (e) Correlation between electronic conductivity calculated using 4-point probe and electrochemical impedance spectroscopy.

The τ_{fit} value vs sample thickness is presented in Fig. 5d (in red). The characteristic time associated with charge/discharge τ corresponds to the minimum charging time at which the electrode can be charged without significant loss in capacity. When operated at charging/discharging times below τ, the sample switch to a resistive behaviour. It shows a small increase from 0.19 s to 0.46 s when the thickness increases from 50 nm to 580 nm. All values are in very good accordance with the ones obtained from electrochemical impedance spectroscopy (τ_{EIS} in black). It indicates that the model proposed here is appropriate to estimate the rate at which the sample is shifting from a capacitive/pseudocapacitive to a resistive behaviour, even for thin film samples. The weak variations of the characteristic time associated with charge/discharge could highlight the fact that the range of thicknesses investigated in the present study should be extended for future works on thicker films.

The increase of τ_{fit} with thickness can be related to the decrease of electronic conductivity previously observed (Fig. 2). As shown in Fig. 5e, the characteristic time associated with charge/discharge τ_{fit} increases with the resistivity, i.e. with the inverse of the conductivity. These results suggest that the characteristic time associated with charge/discharge is governed by the electronic conductivity of the VN electrode and is not diffusion limited. Indeed, the VN thin films have two main roles in the electrodes: it collects and carries electrons as a curent collector and it also stores charges via capacitive, pseudo-capacitive and faradic processes. It can be noted that the VN films are deposited directly on isolating Si/SiO_2 substrates. Hence, the VN needs to conduct electrical charges in-

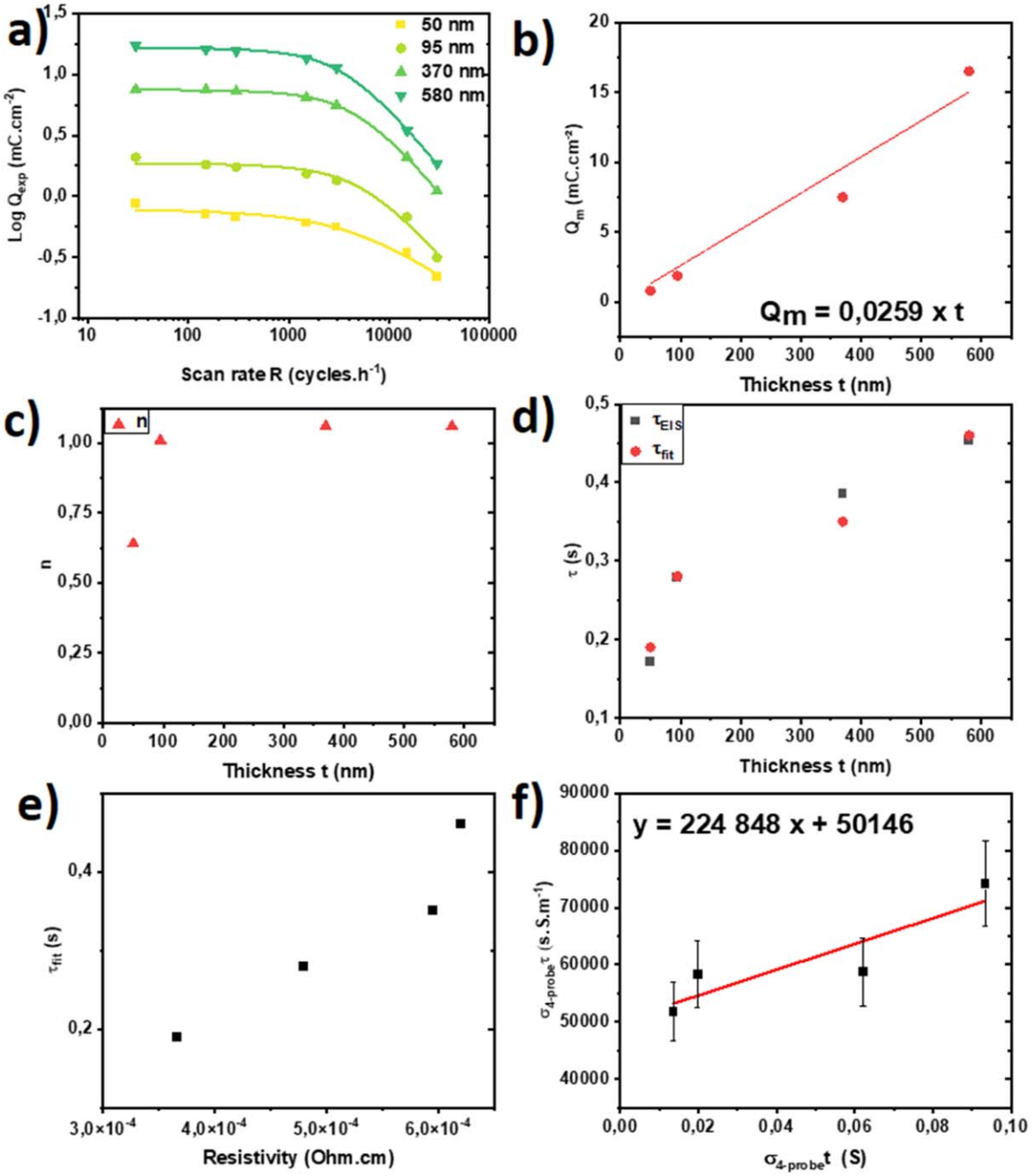

Figure 5. Areal charge density vs scan rate plotted for four different electrode thicknesses. In each case, the solid lines represent fits to Eq. 3. (b) Maximum areal charge using Eq. 3, (c) n value, (d) characteristic times associated with charge/discharge τEIS (in black) and τfit (in red) vs electrode thickness calculated from EIS and Eq. 3 respectively. (e) Evolution of τ vs samples resistivity. (f) Plot of the electrical conductivity of the electrode multiplied by the sample characteristic time associated with charge/discharge τfit vs the electrical conductivity of the electrode multiplied by sample.

plane, all the way to the electrical connexion to the external circuit. Figure 5d clearly shows that its in-plane resistivity needs to be minimized to minimize the characteristic time associated with charge/discharge.

Next, we show that the determination of the characteristic time associated with charge/discharge can be used to evaluate several geometrical and physical properties of the system. As shown in Ref. 25, a supercapacitor can be modelled as a series combination of a resistor and a capacitor, where the resistance includes contributions from the electrolyte and the electrode. Then the characteristic time associated with charge/discharge depends on the volumetric capacitance C_v, the length of the electrode L, the electrode thickness t, the conductance per unit area of the electrolyte G_A, and the in-plane electrode conductivity $\sigma_{4\text{-probe}}$, as shown in Eq. 3.[25]

$$\tau_{fit} = \frac{C_v}{\sigma_{4-\text{probe}}} L^2 + \frac{C_v}{G_A} t \qquad [3]$$

In our case, our different electrode thicknesses lead to different conductivities as well as different values of τ_{Fit}. To deal with this, Eq. 3 can be rewritten as:

$$\sigma_{4-\text{probe}} \tau_{fit} = C_v L^2 + \frac{C_v}{G_A} \sigma_{4-\text{probe}} t \qquad [4]$$

Equation 4 predicts that $\sigma_{4-probe}\tau_{fit}$ scales linearly with $\sigma_{4-probe}t$ (Fig. 5f). Indeed, a well-defined linear trend is observed. The model indicates that the intercept corresponds to C_vL^2 and a value of 5×10^4 s S.m^{-1} is obtained from the linear fit. Previously, C_v was calculated using Fig. 5b, yielding a value of 4.3×10^2 F.cm^{-3}, and with L approximately equal to 1 cm, the calculated C_vL^2 is 4.3×10^4 s S.m^{-1}. Even though a discrepancy of 15% between the fitted and calculated results is observed, the results are very satisfactory.

The model also indicates that the slope is C_V/G_A. The slope obtained by the linear regression in Fig. 5f is determined to be 2.25×10^5 S.m^{-1}. G_A would then equals 1.91×10^3 S.m^{-2}. Knowing that $\sigma_{electrolyte} \approx G_A l$ where $l = 1$ cm is the separation between the working and counter electrodes, the measured $\sigma_{electrolyte}$ equals 19.1 S.m^{-1}. This value closely aligns with the typically reported literature value of $\sigma_{KOH,1M} \approx$20.13 S.m^{-1}[26] at 293 K. This good agreement is further strong evidence that our supercapacitors can be modelled as a series combination of resistor and capacitor (or CPE) and that this model can be used to quantify the rate performance.

In order to confirm that high rate cycling limitations of those samples are mostly due to the RC time constant of the system, which is limited by the resistance of the VN electrode, two samples were prepared: the first one with VN films sputtered on top of a 50 nm thick platinum current collector, and the second one without the Pt current collector, the VN being directly sputtered on Si/SiO_2 substrate. Conductivity of the Pt thin film is 66000 S.cm^{-1}, which is 20 to 30-fold higher than that of VN thin films.

The capacitance vs scan rate, measured with and without a current collector, is shown in Figs. 6 and S3. A clear shift of the curves towards higher scan rates is observed when a platinum current collector is used. Then, Eq. 3 was used once again to fit these measurements. The key impacts of the platinum current collector addition are a decrease in maximum capacity (less than 20%), from 3.48 mC.cm^{-2} to 2.82 mC.cm^{-2}, which could be ascribed to variations in nucleation/growth mechanisms on platinum, a n value close to 1, indicating the rate-limiting processes, are capacitive and or pseudocapacitive processes, and finally an important decrease of the sample characteristic time associated with charge/discharge τ_{fit} from 4.43 s to 0.7 s.

Conclusions

In summary, this study successfully verified the applicability of a semi-empriric model,[25] to assess the rate performance of pseudocapacitive thin film electrodes. The satisfactory outcomes obtained through fitting the model to experimental data enabled the determination of physical properties such as electrolyte conductivity, in good agreement with literature data, strengthening the reliability of the model for the studied thin films.

For vanadium nitride thin films, the primary limitation in high-rate cycling was identified as the electronic conductivity of the electrode. Electrochemical impedance spectroscopy (EIS) and the fitting model were used in good agreement to determine the characteristic time associated with charge/discharge of the samples. It revealed that the overall characteristic time associated with charge/discharge is predominantly governed by the RC time constant of the system. This assertion was substantiated by comparing similar films deposited directly on the isolating substrate or on top of a platinum current collector, resulting in a sixfold decrease in the characteristic time associated with charge/discharge in this last design. This underscores the necessity of employing current collectors, even for pseudocapacitive materials with inherent high electronic conductivity like vanadium nitride if the final application requires high-rate cycling. Further investigations should explore thicker electrodes and alternative pseudocapacitive materials.

Acknowledgements

Labex STORE-EX (ANR-10-LABX-76-01) and Conseil Régional des Pays de la Loire are acknowledged for financial support (PhD grant AL). The research conducted in this publication was jointly funded by the Irish Research Council (IRC), the French Ministries of Europe and Foreign Affairs (MEAE) and Higher Education and Research (MESR) under grant PHC (Partenariat Hubert Curien) Ulysses 2022 entitled "Quantifying the factors limiting rate performance in supercapacitor electrodes").

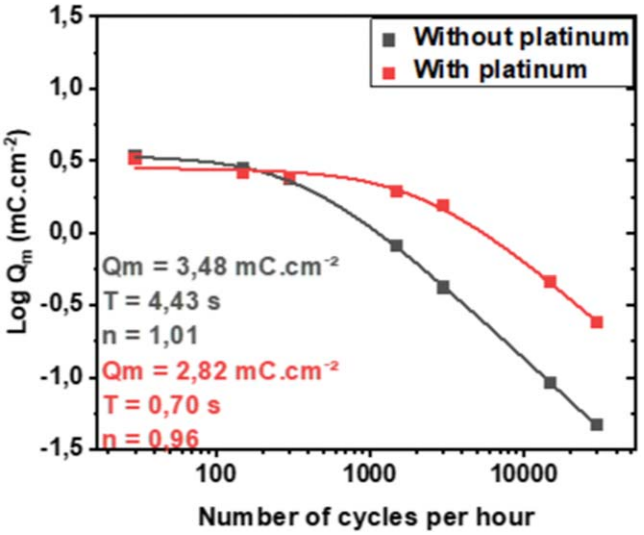

Figure 6. Areal charge vs rate plotted for the samples with and without platinum current collector. The curves are fitted to Eq. 3.

ORCID

Allan Lebreton https://orcid.org/0009-0005-7647-8865
Jérémy Barbé https://orcid.org/0009-0003-3366-4567
Christophe Lethien https://orcid.org/0000-0001-8906-8308
Jonathan N. Coleman https://orcid.org/0000-0001-9659-9721
Thierry Brousse https://orcid.org/0000-0002-1715-0377

References

1. Y. Fu, Y. Peng, L. Zhao, and F. Ran, "Recent advances of fabricating vanadium nitride nanocompositions for high-performance anode materials of supercapacitors." *Journal of Energy Storage. janv*, **75**, 109564 (2024).
2. H.-hui Liu, H.-ling Zhang, H.-bin Xu, T.-ping Lou, Z.-tong Sui, and Y. Zhang, "Influence of the concentration of electrolyte on the capacitive properties of vanadium nitride electrode for electrochemical capacitors." *J. Electrochem. Soc.*, **165**, A97 (2018).
3. E. Le Calvez et al., "Influence of ion implantation on the charge storage mechanism of vanadium nitride pseudocapacitive thin films." *Electrochemistry Communications. avr*, **125**, 107016 (2021).
4. A. Jrondi et al., "Major improvement in the cycling ability of pseudocapacitive vanadium nitride films for micro-supercapacitor." *Adv. Energy Mater.*, 2203462 (2023).
5. Y. Liu, L. Liu, L. Kang, and F. Ran, "Energy storage mechanism of vanadium nitride via intercalating different atomic radius for expanding interplanar spacing." *Energy & Environ Materials*, **5**, 565 (2022).
6. N. Ouldhamadouche et al., "Electrodes based on nano-tree-like vanadium nitride and carbon nanotubes for micro-supercapacitors." *Journal of Materials Science & Technology*, **34**, 976 (2018).
7. A. Achour, R. Lucio-Porto, S. Solaymani, M. Islam, I. Ahmad, and T. Brousse, "Reactive sputtering of vanadium nitride thin films as pseudo-capacitor electrodes for high areal capacitance and cyclic stability." *J Mater Sci: Mater Electron*, **29**, 13125 (2018).
8. O. Bondarchuk, A. Morel, D. Bélanger, E. Goikolea, T. Brousse, and R. Mysyk, "Thin films of pure vanadium nitride: evidence for anomalous non-faradaic capacitance." *J. Power Sources*, **324**, 439 (2016).
9. K. Robert et al., "On chip interdigitated micro-supercapacitors based on sputtered bifunctional vanadium nitride thin films with finely tuned inter- and intracolumnar porosities." *Adv Mater Technol. juill*, **3**, 1800036 (2018).
10. N. Witit-Anun and A. Buranawong, "Effect of sputtering power on the structure of DC magnetron sputtered vanadium nitride thin films." *Journal of Metals, Materials and Minerals*, **27**(1), 47–52 (2017).
11. J. C. Caicedo, G. Zambrano, W. Aperador, L. Escobar-Alarcon, and E. Camps, "Mechanical and electrochemical characterization of vanadium nitride (VN) thin films." *Appl. Surf. Sci.*, **258**, 312 (2011).
12. K. Robert et al., "Novel insights into the charge storage mechanism in pseudocapacitive vanadium nitride thick films for high-performance on-chip micro-supercapacitors." *Energy Environ. Sci.*, **13**, 949 (2020).

13. D. V. Horváth, J. Coelho, R. Tian, V. Nicolosi, and J. N. Coleman, "Quantifying the dependence of battery rate performance on electrode thickness." *ACS Appl. Energy Mater.*, **3**, 10154 (2020).
14. R. Tian et al., "Quantifying the effect of electronic conductivity on the rate performance of nanocomposite battery electrodes." *ACS Appl. Energy Mater.*, **3**, 2966 (2020).
15. R. Tian et al., "Quantifying the factors limiting rate performance in battery electrodes." *Nat. Commun.*, **10**, 1933 (2019).
16. Z. Ling et al., "Quantifying the role of nanotubes in Nano:Nano composite supercapacitor electrodes." *Adv. Energy Mater.*, **8**, 1702364 (2018).
17. S. Deebansok et al., "Capacitive tendency concept alongside supervised machine-learning toward classifying electrochemical behavior of battery and pseudocapacitor materials." *Nat. Commun.*, **15**, 1133 (2024).
18. A. Lebreton et al., "Control of microstructure and composition of reactively sputtered vanadium nitride thin films based on hysteresis curves and application to microsupercapacitors." *Journal of Vacuum Science & Technology A*, **42**, 023405 (2024).
19. A. Morel, Y. Borjon-Piron, R. L. Porto, T. Brousse, and D. Bélanger, "Suitable conditions for the use of vanadium nitride as an electrode for electrochemical capacitor." *J. Electrochem. Soc.*, **163**, A1077 (2016).
20. H. Dinh Khac et al., "Nanofeather ruthenium nitride electrodes for electrochemical capacitors." *Nat Mater [Internet]* (2024), [cité 12 avr 2024]; Disponible sur: https://nature.com/articles/s41563-024-01816-0.
21. D. Choi, G. E. Blomgren, and P. N. Kumta, "Fast and reversible surface redox reaction in nanocrystalline vanadium nitride supercapacitors." *Adv. Mater.*, **18**, 1178 (2006).
22. R. Manjunatha, A. Karajić, H. Teller, K. Nicoara, and A. Schechter, "Electrochemical and chemical instability of vanadium nitride in the synthesis of ammonia directly from nitrogen." *ChemCatChem*, **12**, 438 (2020).
23. E. Haye et al., "Enhancing cycling stability and specific capacitance of vanadium nitride electrodes by tuning electrolyte composition." *J. Electrochem. Soc.*, **169**, 063503 (2022).
24. P. L. Taberna, P. Simon, and J. F. Fauvarque, "Electrochemical characteristics and impedance spectroscopy studies of carbon-carbon supercapacitors." *J. Electrochem. Soc.*, **150**, A292 (2003).
25. T. M. Higgins and J. N. Coleman, "Avoiding resistance limitations in high-performance transparent supercapacitor electrodes based on large-area, high-conductivity PEDOT:PSS films." *ACS Appl. Mater. Interfaces*, **7**, 16495 (2015).
26. R. Gilliam, J. Graydon, D. Kirk, and S. Thorpe, "A review of specific conductivities of potassium hydroxide solutions for various concentrations and temperatures." *Int. J. Hydrogen Energy*, **32**, 359 (2007).